JOURNAL OF APPLIED ELECTROCHEMISTRY **27** (1997) 1184–1192

Effect of bare metal surface on the dissolution in aqueous citrate solutions of magnetite films on carbon steel

I. H. PLONSKI

Institute of Atomic Physics, IFTM, POBox MG-6, Bucharest, Romania

Received 19 April 1994; revised 9 July 1996

The potential–time dependence of magnetite under varying conditions of pH and Fe^{2+} concentration and of magnetite layers on carbon steel with initially exposed small bare metal areas have been studied. The experiments simulate the case of magnetite scales partially removed from surfaces in the course of chemical cleaning when coupling conditions occur with area ratios variable with time. The interpretation is based on an equivalent electric circuit composed of internal current generators of faradaic origin and capacitors simulating the electric double layer at the metal/solution and oxide/solution interfaces.

1. Introduction

Magnetite is the principal corrosion component of sludge, deposits and thick oxide build up on carbon steel components of boilers, heat exchangers and steam generators and on the primary side of heavy water reactors. Acid removal of iron oxide deposits enhances the service life of steel industrial equipment, improves heat transfer, minimizes local corrosion and reduces the radiation field around nuclear power plants. For this reason, many laboratory investigations have been conducted to provide understanding of magnetite and iron dissolution reactions [1–57]. A large amount of work has been focused on the dissolution of free magnetite and the influence of the potential [9, 12, 20, 25, 26, 48], pH [20, 25, 26], redox couples in solution [1, 54, 55], mineral acids [16–18], complexing anions [16–18, 25, 26, 28, 29], temperature [25, 26] and hydrodynamics [25, 26] have been established. However, whether the electron transfer [8, 9], the passage of the reaction products (Fe^{2+}, Fe^{3+}, OH^-) [1, 12, 19, 56] or reactants (H^+, anions) [12, 25, 26, 56] across the double layer, all potential dependent, or the removal of the dissolution products from the reaction site by mass transport, depending on electrode potential, temperature and local hydrodynamic conditions, is the rate determining step for the magnetite dissolution is still a matter of debate [11]. Also, it is far from clear as to the nature of the intermediates formed as a result of the stepwise electron transfer and of the conversion of the oxide lattice in water [12, 49].

Much information is available on the dissolution of oxides from steel surfaces, the manner in which the magnetite dissolution reaction is modified by the presence of the metal substrate and the mutual influence of the oxide on the iron corrosion [2–7, 10–15, 21–24, 27, 31, 32, 35, 38–40, 45, 51–57]. Major contributions are the influence of the oxide layer evolution during dissolution at the open circuit potential of magnetite [8, 9] and the reduction of magnetite supplied by electron source iron dissolution [45].

Operational iron oxide scales contain numerous pores and microcracks [15]. Moreover, concomitantly with chemical and electrochemical dissolution, mechanical detachment of the oxide layer due to the undermining of the base metal occurs [8, 9]. As soon as the solution reaches the metal substrate the iron is oxidized releasing electrons that reduce Fe(III) in the scale [45, 46]; H^+ cross the double layer to react with the oxide ions initially forming OH^-, then H_2O [19].

To simulate some particular situations encountered in the course of actual cleaning, galvanic coupling experiments were performed using spatially separated magnetite and carbon steel coupons. Short-circuited potentials and currents were measured in time, for Fe_3O_4 to Fe area ratios ranging between 0.2 and 7. This is low enough for the resulting galvanic coupling to enter the active region of iron dissolution [8, 9, 12, 45, 53]. An enhanced dissolution of active steel and magnetite, as a result of the galvanic coupling was reported [8, 9]. A similar study, using large Fe_3O_4 to Fe area ratios has been briefly treated [40].

There are similarities and distinctions between a classical external short circuit of two spatially located electrodes and a magnetite on carbon steel single electrode exposing metal surfaces, as is the actual case during oxide removal. Three are mentioned below:

(i) During magnetite dissolution and its mechanical detachment from the metal, an increasing number of alternative Fe and Fe_3O_4 surfaces characterizes this kind of single electrode. The oxide and the metal are initially short circuited; the external galvanic current is zero, but there are local galvanic currents which determine the electrode potential.

(ii) The chemical nature of the so-called electron sink and electron source surface is not always stable with time; under particular conditions

0021-891X

during chemical cleaning, initially or accidentally produced bare metal is recovered by an oxide.

(iii) The potential drop in the solution is much greater when the electrodes are spatially separated and cannot be neglected in such a case.

This paper reports on the behaviour of the pseudo-galvanic, heterogeneous, electrode obtained by a controlled scratching of the magnetite layer in order that a definite small area in comparision with the oxide areas is exposed at immersion time. Additional experiments on pure magnetite and carbon steel were performed, thus covering the real situations encountered during chemical cleaning, thus helping to define oxide on carbon steel dissolution chemistry.

2. Experimental details

2.1. *Materials*

2.1.1. Carbon steel working electrode (*CS*). Small cylinders of 11 mm diameter, 5 mm height and 173 mm^2 lateral area were cut from a rod of carbon steel OL 45 (C 0.42...0.50, Mn 0.50...0.90, Si 0.17...0.37, P max 0.04, S max 0.05 all in wt %), Romanian Technical Standard STAS 880–08 equivalent to AISI 1045. The samples were mechanically polished, chemically etched with boiling 10% HCl for 3 min, washed with distilled water, then finally rinsed and boiled for 15 min in acetone.

2.1.2. Magnetite on carbon steel electrode (*CS*/Fe_3O_4). Cylinders of OL 45 carbon steel, prepared as above, were oxidized for 21 days in LiOH aqueous solution, pH 10.5, in a passivated stainless steel autoclave, thermostated to 333 ± 3 °C, pressurized with D_2 to 96 ± 2 atm. The thickness and composition of the oxide layer were established from X-ray diffractometry data. The morphology of the film was determined by scanning electron microscopy (SEM). After autoclaving for 48 h, the only phase that could be detected was magnetite. The resulting duplex layer, of 2.0 ± 0.2 mm thickness, consisted of an outer layer of spherical monocrystals and crystallites, and a porous base layer.

2.1.3. Solid magnetite electrode (*MG*). This was 2.3 mm thick, 11 mm wide, 81 mm long and obtained by high temperature acidic corrosion of 1 mm thick carbon steel coupons. Oxidation throughout the whole sample thickness was achieved within 408 h at 320 °C in 1 g dm^{-3} Cl^- as NaCl adjusted initially to room temperature and pH 2 by HCl addition [8, 9].

2.1.4. Composite samples simulating pseudo-galvanic coupling. Composite samples between carbon steel and magnetite were obtained by mechanical removal of the oxide layer in order to expose four metal areas of roughly (mm^2): 0.02, 0.1, 0.2 and 1. To obtain these bare metal surfaces, one to four scratches of various width were made at equal distances. The area of these metal strips was determined using a magnifying glass.

2.2. *Solutions*

Complex buffer solutions of 0.1 M HCl and 0.1 M disodium citrate (Na_2HCit) were mixed to obtain pH of 2.3 and 4.1. Complexing buffer solutions of 0.1 M citric acid (H_3Cit) and 0.1 M disodium citrate were mixed to obtain pH of 1.9, 3.8 and 4.8.

Complexing buffer solutions of 0.1 M citric acid and 0.1 M disodium citrate pH 3.8 and 0.1 M ferrous citrate (FeHCit) were mixed to obtain total iron concentration between 4.8×10^{-6} and 4.1×10^{-4} M.

2.3. *Facilities and experimental setup*

The experiments were performed in a 250 ml thermostated cell. The carbon steel and magnetite on carbon steel specimens were mounted in an electrode holder between two area limiting PTFE gaskets so that only the lateral area of the cylinder was in contact with the solution. Magnetite plaquettes were placed in a vertical position.

The experiments were conducted at 35 °C. Two hours before electrode immersion and during the measurements, the solution was purged and stirred by nitrogen or hydrogen bubbling. No notable effect of the nature of the inert gas on the rest potential value was observed. Some experiments were performed under static conditions.

The potential difference between the working and SCE reference electrodes was measured at open circuit using a digital millivoltmeter (input impedance 10^{12} Ω) starting 5 s after immersion.

3. Results and discussions

3.1. *Carbon steel, pure magnetite and magnetite on carbon steel electrodes*

Figure 1 shows the potential–time curves for carbon steel (CS), magnetite (MG) and magnetite on carbon steel (CS/Fe_3O_4) at 35 °C, as function of pH [35].

A typical curve for Fe_3O_4 on Fe in EDTA pH 3.3 at 21 °C, reported by Shoesmith [50] is superimposed. In the absence of a metallic support (i.e. on pure magnetite) the electrode potential has very positive values randomly distributed between 570 and 700 mV vs NHE, irrespective of the pH in the range between 2.2 and 4.8. Such a positive value can be attributed to the solid system of high reversibility $Fe_3O_4/\gamma Fe_2O_3$ arising from the superficial oxidation of magnetite prior to immersion [10, 30, 52]. Hickling and Ives [20] reported a static potential of all iron oxides containing Fe(III) in 0.5 M H_2SO_4 between 600 and 700 mV vs NHE. The influence of pH on magnetite solubilization in EDTA based solutions has been assessed by electrochemical measures after completion of 3 or 4 h test and verified by Fe_3O_4 weight losses by Brunet

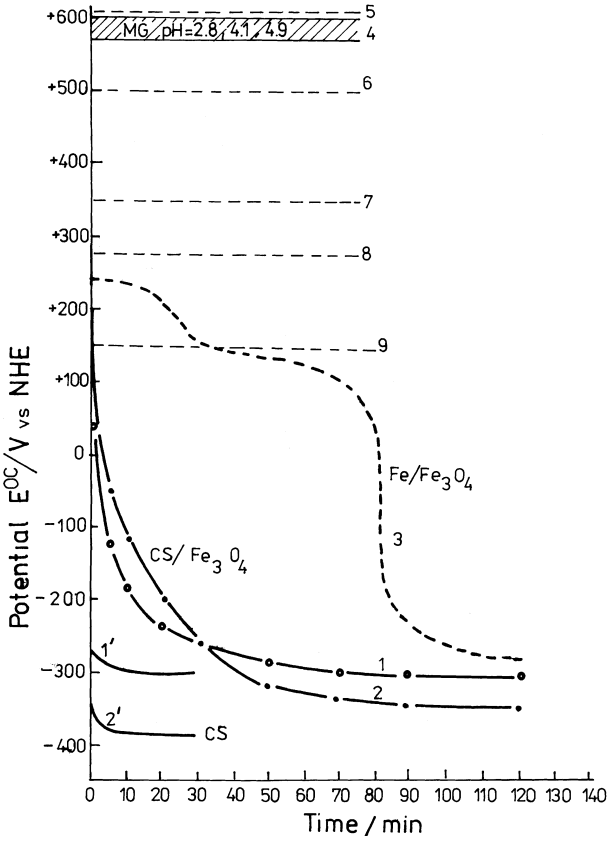

Fig. 1. Time-dependence of open-circuit potential of carbon steel (CS), magnetite (MG) and magnetite on carbon steel (CS/Fe_3O_4) as function of pH, at 35 °C, under nitrogen atmosphere. Typical curve for Fe_3O_4 on Fe in EDTA pH 3.3 at 21 °C reported in [50], and open circuit potentials for magnetite in some mineral and complexing acid solutions of different pH, taken from the literature, are superimposed.
Curves 1, 1′, 2, 2′, 4: 0.1 M HCl + 0.1 M NaHCit.
CS/Fe_3O_4: (1) pH 2.36; (2) pH 4.11, [35].
CS: (1′) pH 2.36; (2′) pH 4.11, [35].
(3) Fe/Fe_3O_4/EDTA pH 3.3 [50].
(4) Hatched region: MG, pH 2.8, 4.1, 4.9, (this paper).
(5) MG/H_2SO_4 pH 0.5, [20].
(6) MG/H_3Cit pH 3.5, [32].
(7) Fe_3O_4/$HClO_4$ pH 2.8, [26].
(8) Fe_3O_4/H_3Cit + EDTA pH 3.5, [32].
(9) Fe_3O_4/EDTA pH 3.0, [26].

et al. [8, 9]. The authors found that the maximum solubilization rates measured by c.d. plateaux are insensitive to pH. Also, no pH influence on the open circuit potential of compact magnetite on carbon steel in acid complexing electrolytes has been observed by Shoesmith *et al.* as long as the $E^{OC}_{Fe_3O_4/Fe} - t$ system did not enter the region of sharp decrease [50, 51].

The influence of total iron in solution, that is, Fe^{2+} and Fe(II) (citrate complexes) on the pure magnetite potential is depicted in Fig. 2. A shift towards negative values with increase in the bivalent iron concentration corroborates qualitatively the observations of Engell [12] and emphasizes the participation of this ion in the potential determining reactions [1].

Figure 1 also shows that when the metal substrate is present, the initial open circuit potential is always more negative than that of the free magnetite; this supports the Frenier and Growcock [15] idea that all magnetite layers grown on ferrous alloy surfaces contain a number of microcracks at the bottom of which additional anodic reactions take place. Rationally, this leads to the conclusion that the initial potential of the magnetite layer depends in a complex way on the metallic surface area, free or in a low oxidation state.

Thus, the typical sigmoid shaped curve of Shoesmith [50], obtained with partially protective magnetite grown on iron support by oxidation in 0.5 M NaOH at 280 °C, displays a potential value between 100 and 200 mV vs NHE stabilized over at least 1 h. In our experiments performed with CS/Fe_3O_4 samples, prepared by oxidation in 10^{-4} M LiOH (a less aggressive pH), no plateau occurs. The potential immediately enters the region of sharp decrease, which lasts about 1 min, then moves slowly toward a value corresponding to carbon steel free corrosion. The initial value obtained by extrapolation of the *E/t* curves to $t \rightarrow 0$ approaches the plateau of Fe/Fe_3O_4, but the potential measured 5 s after immersion is situated at more negative values and depends on pH. This characterizes a nonprotective oxide layer exhibiting, from the beginning, a large number of microcracks, pores, scratches, or other kinds of defects communicating with the metal surface.

All *E*/*t* curves have a negative slope d*E*/d*t*. An electrode at open circuit charges with negative charges only as a result of the predominance of the local electron source reactions over the electron sink ones.

In the region of the sharp decrease of open potential at potentials more positive than the equilibrium potential of the hydrogen electrode, the greater the pH the more positive the potential, that is, d*E*/d pH > 0. This behaviour has been qualitatively confirmed with a good reproducibility using four pH values within the range 2.2 to 4.8 and two magnetite on CS samples per condition. This is explained by the fact that the potential value in this region termed the 'transition range of active iron dissolution' [23], is indirectly controlled by the large increase in metal to oxide area ratio via chemical and electrochemical oxide dissolution, both favoured by decreasing pH. The anodic process prevailing on the metal surface is oxide species formation [44], for instance

$$Fe + H_2O \rightarrow FeO + 2e^- + 2H^+ \qquad (1)$$

and

$$3Fe + 4H_2O \rightarrow Fe_3O_4 + 8e^- + 8H^+ \qquad (2)$$

occurring concomitantly with cathodic magnetite reduction according with the global reaction

$$Fe_3O_4 + 2e^- + 8H^+ \rightarrow Fe^{2+} + 4H_2O \qquad (3)$$

which undoubtedly proceeds stepwise.

Reaction 1 is followed by chemical oxide dissolution

$$FeO + 2H^+ \rightarrow Fe^{2+} + H_2O \qquad (4)$$

and/or further oxidation

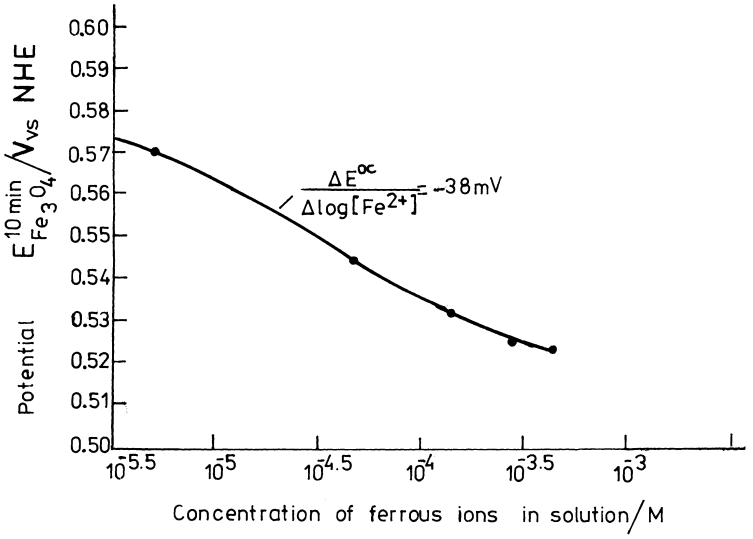

Fig. 2. Effect of total iron concentration in the range 4.8×10^{-6} M through 4.1×10^{-4} M as Fe(II) citrate on the open circuit potential of magnetite in 0.1 M citric acid + 0.1 M disodium citrate, pH 3.8, at 36 °C, under hydrogen bubbling.

$$FeO + H_2O \rightarrow FeOOH + e^- + H^+ \quad (5)$$

$$3FeO + H_2O \rightarrow Fe_3O_4 + 2e^- + 2H^+ \quad (6)$$

In the region of slow potential decrease, at potentials more negative than the equilibrium potential of the hydrogen electrode, that is, in the 'active range of active iron dissolution' [23], the slope dE/d pH is negative, therefore characteristic of active iron corrosion in acid media. In this case, the predominant reactions on the metal surface are iron dissolution

$$Fe \rightarrow Fe^{2+} + 2e^- \quad (7)$$

and hydrogen evolution, described by the overall reaction

$$2H^+ + 2e^- \rightarrow H_2 \quad (8)$$

In this region the potential is more negative and the ratio $A_{Fe}/A_{Fe_3O_4}$ increases slowly so that the free metal area is large enough for the current associated with Reactions 6 and 7 to prevail over the current due to Reactions 1, 2 and 3.

3.2. *Pseudogalvanic coupling between carbon steel and magnetite to carbon steel*

In Fig. 3, the time evolution of the open circuit potential in a solution with pH 4.1 is plotted for various initial metal-to-magnetite surface area ratios. On the same graph, the potential–time dependence for CS/Fe_3O_4 (curve 1) and CS (curve 6) electrodes, as well as for compact nonporous (curve 1′) and porous base magnetite layer (curve 2′) taken from [51] are superimposed. The equilibrium potentials, E^O, for the thermodynamically possible reactions at $a_{Fe^{2+}} = 10^6$ M and $p_{H_2} = 1$ atm [44] are written on the right hand side of the Figure.

From these curves following observations may be made:

(i) Five seconds after the immersion moment, the electrode potential and the slope dE/dt are more negative the greater the bare metal area.

(ii) For a small initial free metal area, when the initial potential is more positive than the equilibrium potential of the hydrogen evolution reaction (curves 2, 3 and 4), the potential decreases to a minimum whose value is always above the equilibrium potential of the Fe/Fe_3O_4 or Fe/FeO systems, then increases to a maximum whose value is approximately equal to the potential value which the CS/Fe_3O_4 electrode would have in the absence of the initial free metal (curve 1). The potential then decreases towards the CS electrode potential.

The minima and maxima in potential are more negative and delayed the greater the initial free metal area. The smaller the ratio $A^i_{Fe}/A^i_{Fe_3O_4}$ the smaller the difference $E^{max}-E^{min}$. Removal of the electrode from the solution when the potential reaches its maximum value showed that the initial bare metal surface was again covered by a black oxide.

(iii) If the initial bare metal area is sufficiently large (curve 5) so that the potential has an initial value more negative than the equilibrium potential of the H^+/H_2 electrode, the E/t wave develops a plateau which lasts until curve 1 is reached. Thereafter, the two curves proceed roughly in parallel. This may be due to the fact that as soon as the hydrogen ions are discharged on the metal, the resulting atomic and molecular hydrogen blocks the iron surface [34, 36, 37, 41, 42], protecting it against reoxidation through Reactions 1 and 2. Concomitantly, the atomic and molecular hydrogen diffuses toward the oxide increasing its dissolution through a reductive mechanism.

(iv) Extrapolation of the remark (ii) to the limit $A^i_{Fe}/A^i_{Fe_3O_4}$ leads to the conclusion that when the initial bare metal surface is small, the wave turns

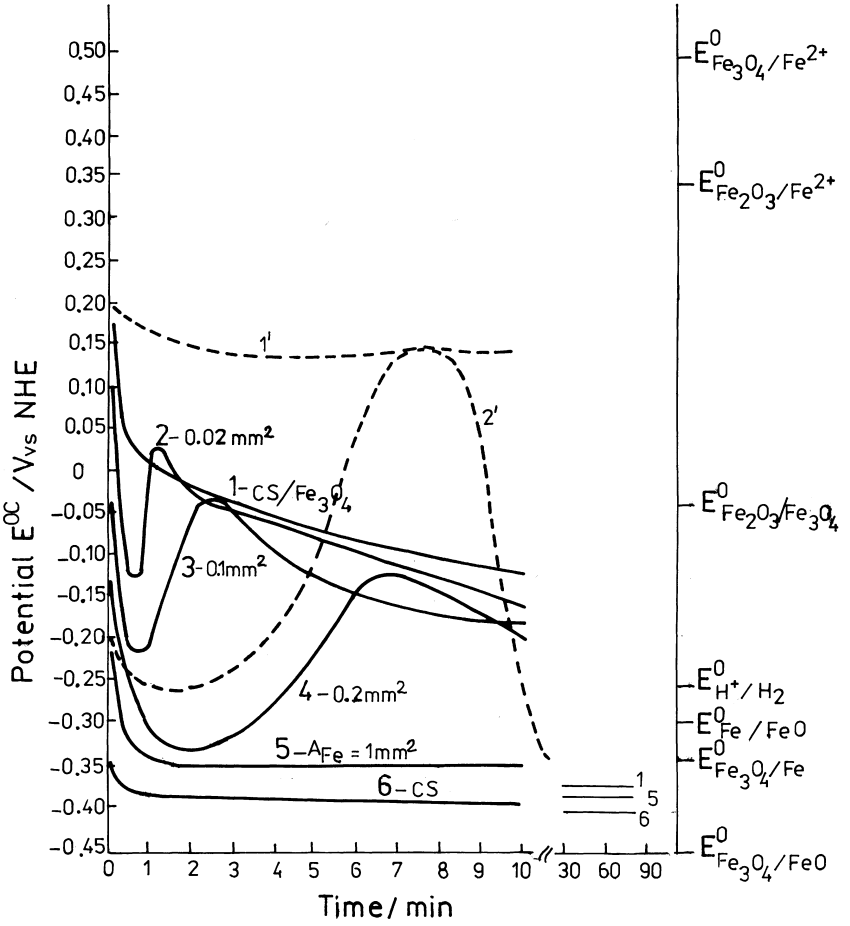

Fig. 3. Time-dependence of the open-circuit potential of carbon steel (curve 1), magnetite on carbon steel (curve 6) and of pseudo-galvanic coupling between magnetite and carbon steel in 0.1 M HCl + 0.1 M disodium citrate, pH 4.1, at 35 °C, under nitrogen atmosphere and static condition, for various ratios between geometrical initial free metal and oxide layer areas $A_{Fe}(mm^2)/A_{Fe_3O_4}(mm^2)$: curve (2) 0.02/173; curve (3) 0.1/173; curve (4) 0.2/173; curve (5) 1/172; (1′) porous, (2′) nonporous magnetite layer [51].

into a monotonically decreasing *E*/*t* curve superimposed on curve 1, when a porous, penetrable layer is present, and into a sigmoid curve for more compact layers. The extrapolation of the remark (iii) for very high values of the ratio $A^i_{Fe}/A^i_{Fe_3O_4}$ again leads to the conclusion that the *E*/*t* wave becomes a monotonically decreasing *E*/*t* curve, approaching curve 6.

(v) When Fe_3O_4-on-CS enters in the region of sharp potential decrease, the time taken to complete oxide dissolution is little altered by the sudden presence of the bare metal. This statement is based on the fact that the final parts of all *E*/*t* curves practically coincide. It appears that the existence of the bare metal and the reactions occurring on it have no detectable influence on the opening of the pores and generally on the oxide dissolution from the covered surface.

4. Theoretical treatment

4.1. *Fundamentals*

The transient regime of the open circuit potential of a composite, heterogeneous electrode from the moment of immersion in the solution until the steady state is reached can be approached through the equivalent circuit shown in Fig. 4 where (a) C_{Me} and C_{Ox} are electric capacitors simulating metal/solution and magnetite/solution double layers, characterized by the differential capacity C_{Fe} and $C_{Fe_3O_4}$ and by the area of the capacitor plates A_{Fe} and $A_{Fe_3O_4}$, respectivley, and (b) the capacitors are charged by the time-dependent internal sources of faradaic origin G^{INT}_{ox} and G^{INT}_{Me} which supply the electrode system with the net currents resulted from the electrochemical reactions occurring at the magnetite surface, $I^{Ox}_F(t)$, and at the metal surface, $I^{Me}_F(t)$. The galvanic coupling potential, E^{GC}, is measured against a reference electrode situated in solution at a distance equivalent to the resistance r_1. The currents charging the capacitors C_{Ox} and C_{Me} are I^{Ox}_{DL} and I^{Me}_{DL}, respectively. According to Kirchoff's law

$$I^{Ox}_{DL} = I^{Ox}_F(t) - I_1(t), \quad I^{Me}_{DL} = I^{Me}_F(t) - I_2(t) \qquad (9)$$

and

$$E_{Me/Sol} = E_{Me/Sol} - I_2 r_0 \qquad (10)$$

At the steady state, $I^{Ox}_{DL} = I^{Me}_{DL} = 0$, the galvanic coupling current is $I^{GC} = I^{Ox}_F = I^{Me}_F$.

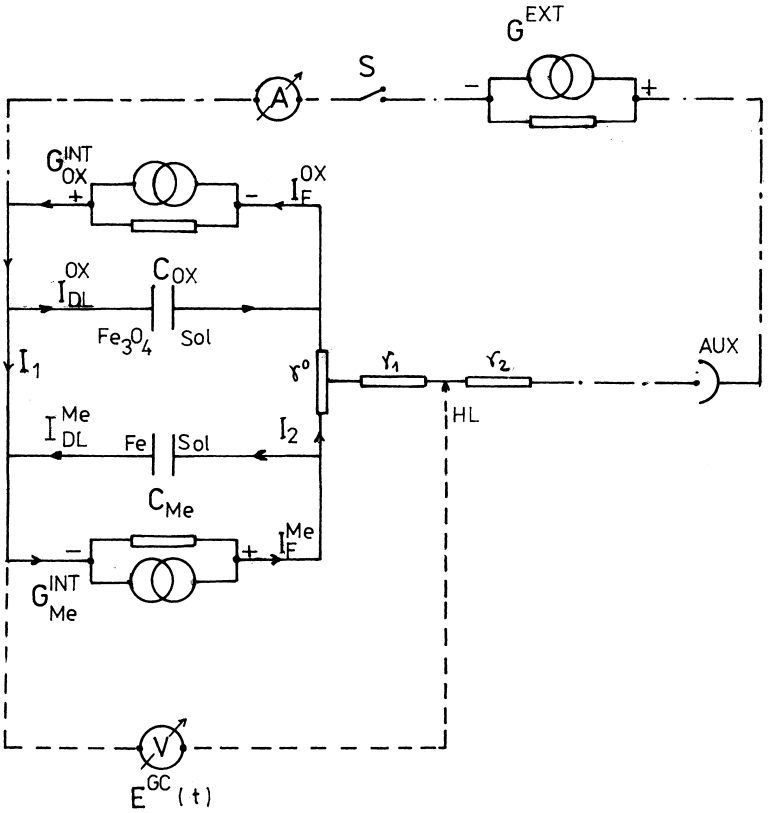

Fig. 4. Equivalent electric circuit simulating the charging of the magnetite/solution/metal interfaces: C_{Me} = free metal/solution capacitor; C_{ox} = oxide/solution capacitor; G_{Me}^{INT} and G_{Ox}^{INT} = internal sources generating the net current resulted from electrochemical reactions occurring on the metal, I_F^{Me}, and magnetite surface, I_F^{Ox}, respectively. r_0 = the solution resistance between the magnetite and iron; $I_{DL}^{Ox} = I_F^{Ox}(t) - I_1(t)$, $I_{DL}^{Me} = I_F^{Me}(t) - I_2(t)$, and $E_{Me/Sol} = E_{Me/Sol} - I_2 r_0$. At the steady state the charging currents $I_{DL}^{Ox} = I_{DL}^{Me} = 0$, and the galvanic coupling current, $I^{GC} = I_F^{Ox} = I_F^{Me}$. Key: (——) internally short circuit metal/oxide under open circuit; (- - - -) potential measurement; (—.—.—) polarization circuit; (S) switch; (Aux) auxiliary electrode; (A) ammeter; (V) voltmeter.

To underline the difference between the internal and the external current sources, the dotted-dashed lines designs the interrupted external polarization circuit where G^{EXT} is current source and r_2 is the resistor equivalent to the solution resistance between the auxiliary electrode, AUX, and the tip of the Haber–Luggin capillary. (As usual, the exceedingly minuscule leakage current across the high impedence voltmeter, V, and the reference electrode can be neglected).

For comparison, Fig. 5. shows the equivalent circuit of a metal/metal ions electrode system under open circuit conditions; $E(t)$ is the transient of the open circuit potential against a reference electrode. The equivalent capacitor of the double layer, C_{DL}, is charged by the time-dependent faradaic internal sources, G_A^{INT} (associated to $Me \rightarrow Me^{z+} + ze^-$) and G_C^{INT} (associated to $Me^{z+} + ze^- \rightarrow Me$) which supply the net charging current $I_{DL} = I_C - I_A$. At the equilibrium, $I_{DL} = 0$ and $I_C = I_A = I^O$ so that the exchange current, I^O, flows in both directions through the resistors R_A and R_C equivalent to the internal resistances of the two equivalent generators G_A^{INT} and G_C^{INT}, respectively.

If in Fig. 4 r_0 is zero, the reactions at oxide/solution and metal/solution interfaces evolve at the same potential and the kinetic equations can be treated analogously with those established for reactions occurring at the mixed potential under open circuit conditions, E^{OC}, that is, $E^{GC} = E^{OC}$. This is the case where the hydrogen evolution reaction replaces the magnetite reduction reaction.

Whether the potential drop across r_0 is or is not negligible depends on the galvanic couple geometry, that is, the distance between the electron sink and source surfaces and their areas, the electrolyte resistance and the magnitude of the time-dependent galvanic current, I^{GC}. Obviously, the assumption $E^{GC} = E^{OC}$, that is, the potential difference across the metal–electrolyte interface at the electron source metal surface of the internal short-circuited equivalent cell is virtually equal to that at the electron sink oxide surface, requires that the intermetal-oxide surfaces be small, that the electrolyte be high conducting, the difference between the stationary open circuit potential of the isolated oxide and iron be small, and the galvanic current be small. (To make a comparison, one passes from the local cell to the mixed potential corrosion theory.)

The relationship between the areas of the metal and oxide is very important. On one hand, the corrosion rate of an *active* metal is dependent upon the current density; this is higher if the area of the active metal is small compared to that of the oxide and can lead to local pitting corrosion. On the other hand, the steady state mixed potential establishes at a value depending on the equality between the current intensities associated with the electron source and electron sink reactions. For example, for the global reactions of iron

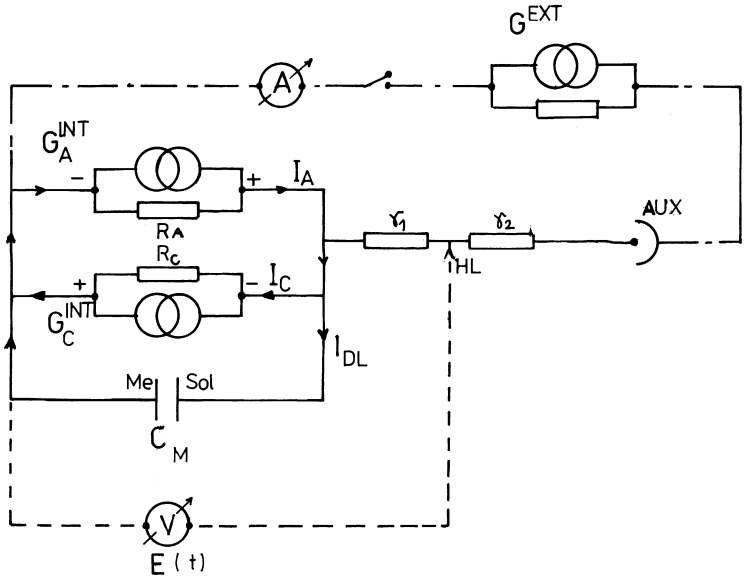

Fig. 5. Equivalent circuit of a metal/metal ions electrode system under open circuit conditions; $E(t)$: transient of open circuit potential against a reference electrode; C_{DL}: equivalent capacitor of double layer charged by time-dependent faradaic internal sources, G_A^{INT} (associated to $Me \rightarrow Me^{z+} + ze^-$) and $G_C{}^{INT}$ (associated to $Me^{z+} + ze^- \rightarrow Me$) which supply the net charging current $I_{DL} = I_C - I_A$. At equilibrium, $I_{DL} = 0$ and $I_C = I_A = I^O$ so that the exchange current, I^O, flows in both directions through resistors R_A and R_C equivalent to internal resistances of the two equivalent generators G_A^{INT} and G_C^{INT}, respectively.

dissolution and magnetite reduction, the open circuit mixed potential results from the equality

$$2FA_{Fe}k_{a,Fe}\exp(2\alpha E^{OC}) = 2FA_{Fe_3O_4}k_{c,Fe_3O_4}(a_{H^+})^8\exp(-2\alpha E^{OC}) \quad (11)$$

where A_{Fe} and $A_{Fe_3O_4}$ are the metal and magnetite surface areas, respectively, $k_{a,Fe}$ and k_{c,Fe_3O_4} are electrochemical rate constants, and $\alpha = F/2RT$. The result is

$$4\alpha\, E^{OC} = [A_{Fe_3O_4}k_{c,Fe_3O_4}(a_{H^+})^8] : [A_{Fe}k_{a,Fe}] \quad (12)$$

from which it can be seen that the mixed potential (or the corresponding galvanic coupling potential) is the more positive the smaller the metal area in comparison with the exposed oxide area. This can lead the metal to leave the active region and enter the prepassive or passive region. Consequently, the metal corrosion rate decreases under coupled conditions compared to non-coupled conditions.

4.2. *Kinetics*

For simplicity, in the derivation below it is assumed that the potential difference owing to Fe/Fe_3O_4 contact, the resistance of the oxide film and r_0 are negligible. In this case, the differential equivalent capacity of the composite electrode C_{DL} is given by

$$C_{DL} = (A_{Fe}C_{Fe} + A_{Fe_3O_4}C_{Fe_3O_4}) : (A_{Fe} + A_{Fe_3O_4}) \quad (13)$$

where the metal and the oxide area, A_{Fe} and $A_{Fe_3O_4}$, respectively, are time-dependent. Consequently, the kinetic equation describing the charging of the double layer capacity concomitantly with establishing the electrode potential, E, against the reference potential, E_{ref}, can be written as

$$(A_{Fe} + A_{Fe_3O_4})C_{DL}\frac{d(E - E_{ref})}{dt} = A_{Fe}\sum I_{Fe} + A_{Fe_3O_4}\sum I_{Fe_3O_4} \quad (14)$$

where $\sum I_{Fe}$ and $\sum I_{Fe_3O_4}$ represent the sum of the faradaic currents associated with the electrochemical reactions occurring on the metal and on the oxide surface, respectively, and t is the time.

Here the characteristic points at minimum and maximum of the $(E - E_{ref})/t$ curve are considered for which

$$\frac{d(E - E_{ref})}{dt} = 0 \quad (15)$$

This discussion will be confined to electrodes displaying a minimum above the equilibrium potential of hydrogen reaction so that this last process can be neglected.

Therefore, for the composite electrode, the following processes are taken into account in the potential region under discussion: iron dissolution and oxide formation according to Reaction 7 and 1, respectively, on the bare metal surface and the first stage of magnetite reduction (Reaction 3)

$$Fe_3O_4 + e^- + H^+ \rightarrow Fe_3O_4H \quad (16)$$

hypothetically assumed as the rate determining step, occurring on the oxide surface.

During this treatment, the following notation will be used:

$A_{Fe}^i, A_{Fe}^{min}, A_{Fe}^{max}$ = bare metal area at immersion time, at minimum and maximum, respectively,

$A_{Fe_3O_4}^i$ = initial oxide surface area

$k_{Fe^{2+}}, k_{Fe/FeO}, k_{Fe_3O_4/Fe^{2+}}$ = the electrochemical rate constant of Reaction 7, 1 and 3, respectively, and

$\alpha = F/2RT$, where F, R and T have the usual meaning.

Because, from Fig. 3, the curves which have minima at potentials more positive than the equilibrium potential of the hydrogen electrode have maxima at times shorter than 3 min, we estimate that the free metal surface area changes abruptly but the oxide surface area varies slowly enough to be considered approximately constant.

Thus, the faradaic current intensity associated with the above mentioned reactions is given by

$$I_F = 2FA_{Fe}^{min}(k_{Fe^{2+}} + k_{Fe/FeO})\exp(2\alpha E^{min}) - A^{i}_{Fe_3O_4}k_{Fe_3O_4/Fe^{2+}} \times a_{H^+}\exp(-\alpha E^{min}) \quad (17)$$

for $E = E^{min}$, and by

$$I_F = 2FA_{Fe}^{max}(k_{Fe^{2+}} + k_{Fe/FeO})\exp(2\alpha E^{max}) - A^{i}_{Fe_3O_4}k_{Fe_3O_4/Fe^{2+}} \times a_{H^+}\exp(-\alpha E^{max}) \quad (18)$$

for $E = E^{max}$.

Combining Equations 14, 15, 17 and 18 gives

$$E^{min} = \ln[(A^{i}_{Fe_3O_4}k_{Fe_3O_4/Fe^{2+}} \times a_{H^+}) \div (2A_{Fe}^{min}(k_{Fe^{2+}} + k_{Fe/FeO})]/3\alpha \quad (19)$$

and

$$E^{max} = \ln[(A^{i}_{Fe_3O_4}k_{Fe_3O_4/Fe^{2+}} \times a_{H^+}) \div (2A_{Fe}^{max}(k_{Fe^{2+}} + k_{Fe/FeO})]/3\alpha \quad (20)$$

By subtracting Equation 19 from Equation 16 and recalling the expression for α, the ratio between the bare metal area at minima and maxima of the potential–time curve becomes

$$A_{Fe}^{min}/A_{Fe}^{max} = \exp[3F(E^{max} - E^{min})/2RT] \quad (21)$$

By substituting the experimental difference $(E^{max} - E^{min})$ taken from curve 2, Fig. 3, in Equation 21, a value $A_{Fe}^{min}/A_{Fe}^{max}$ of about 10^4 is obtained, which means that the free metal area is orders of magnitude lower at the maximum than at the minimum of the E/t curve. This result is in agreement with the experimental observation that in this region of potential the initial free metal surface is recovered by an oxide, a phenomenon by which the bare metal area continuously decreases.

5. Conclusions

The following points can now be made:

(i) Magnetite layers built up on ferrous metal support in aqueous solutions are always heterogeneous electrodes initially exposing a large surface area of compact, coherent, magnetite and a small surface area of rapidly soluble thin oxide, most probably in a low oxidation state, covering the metal surface at the base of pores, cracks and other faults.

(ii) The initial value of the open circuit potential of this heterogeneous electrode is more negative with respect to the pure magnetite potential the greater the initial ratio between the base of the faults and the compact oxide layer surface areas.

(iii) When the compact magnetite layer is damaged to such an extent that, before the system enters the region of potential sharp decrease, some superficially oxidized or free metal is exposed to solution attack, the initial value of the potential, as well as the trend of the potential–time curve, depends on the ratio between the metal and the compact oxide surface areas.

(iv) If the initial open circuit potential is more positive than the equilibrium potential of the hydrogen electrode, the anodic iron oxide formation runs in parallel with iron dissolution in supplying electrons for magnetite reduction. The initial bare metal is recovered by black oxide and the potential–time curve is wave-shaped. After the maximum of the wave, the potential declines similarly to the usual undamaged magnetite on carbon steel. From the practical standpoint, this means that there is no real condition for local corrosion in this case.

(v) If the initial open circuit potential of this composite electrode is more negative with respect to the equilibrium potential of the hydrogen electrode, the oxide dissolution and the increase in bare metal surface prevail, and the potential—time curve decreases monotonically similarly to the case of carbon steel electrodes.

(vi) When, during chemical cleaning, galvanic coupling is used to enhance the oxide removal, the metal to oxide surface area must be large enough to cause the system to enter the potential region of monotonically potential decrease.

Acknowledgements

Pure magnetite coupons were generously offered by Dr G. Pinard-Legry and Dr Solange Brunet, Centre d' Etudes et de Recherches sur les Matériaux, Fontenay aux Roses, France.

References

[1] E. Baumgartner, M. A. Blesa, H. A. Marinovich and A. J. G. Maroto, *Inorg. Chem.* **22** (1983) 2226.
[2] W. Bell, *in* ASME Publication, Nov.–Dec. (1960), paper 60-WA-257.
[3] P. Berge, C. Ribon and P. Saint-Paul, The International 7th Corrosion Forum for the Protection and Performance of Materials, Palmer House, Chicago (1974).
[4] D. M. Blacke, J. Engle and C. A. Lesinski, *in* Proceeding of the International Water Conference, Pittsburg, (1962), p. 135.
[5] W. J. Blume, *Mater. Performance* **3** (1977) 15.
[6] J. Brown, D. G. Kingerley, V. Ashworth and M. J. Willett, *Chemistry and Industry*, Sept. (1969) 35.
[7] J. Brown, D. G. Kingerley and M. J. Louster, *Br. Corros. J.* **13** (1978) 93.
[8] S. Brunet and G. Turluer, *in* Proceedings of the 5th European Symposium on Corrosion Inhibitors, Italy, Ferrara, Sept. (1980) p. 513.
[9] S. Brunet, G. Pinard-Legry and G. Turluer, *in* Proceedings of the 8th International Congress on Metallic Corrosion, Germany, Frankfurt am Main, Dechema (1981) p. 1634.

[10] K. E. Buob, A. F. Beck and M. Cohen, *J. Electrochem. Soc.* **105** (1958) 74.
[11] J. W. Diggle, *in* 'Dissolution of Oxide Phases from Oxides and Oxides Films', vol. 2 (edited by J. W. Diggle) Marcel Dekker, New York (1973) p. 281.
[12] H. J. Engell, *Z. Phys. Chem.* **7** (1956) 158.
[13] M. Fields, Proceedings of the 2nd International Conference on Metal Corrosion, NACE, Houston, Texas (1963).
[14] W. W. Frenier, *Corrosion* **40** (1984) 176.
[15] W. W. Frenier and F. B. Growcock, *ibid.* **40** (1984) 663.
[16] I. G. Gorichev, *Werkst. Korros.* **30** (1979) 426.
[17] I. G. Goricev and N. A. Kapriyanov, *J. Appl. Chem. USSR* **52** (1979) 473.
[18] I. G. Gorichev *et al., Russ. J. Phys. Chem.* (trans. from *Zh. Fiz. Khim.*) **50** (1976) 1853; *ibid.* **52** (1978) 681; *ibid.* **53** (1979) 1293; *ibid.* **54** (1980) 774.
[19] S. Haruyama and K. Masamura, *Corros. Sci.* **17** (1978) 263.
[20] A. Hickling and D.J.G. Ives, *Electrochim. Acta* **26** (1975) 63.
[21] J. Kertesz and I. H. Plonski, *Patent RO-OSIM, 149 080* (1992) Romania.
[22] W. S. Leedy, *in* EPRI, ASME, OSU, Seminar on Decontamination of Nuclear Plants (1975).
[23] W. Lorenz and K. Heusler, in 'Corrosion Mechanisms', (edited by F. Mansfeld) Marcel Dekker, New York (1987) p. 4.
[24] C. M. Loucks, 'Power', McGraw-Hill, New York (1961).
[25] D. S. Mancey, D. W. Shoesmith, J. Lipkowski, A. C. McBride and J. Noël, *J. Electrochem. Soc.* **140** (1993) 637.
[26] D. S. Mancey and A. C. McBride, Report IAEA —TECDOC —716, 'Decontamination and decommissioning of nuclear facilities', Aug. (1993) pp. 13–33.
[27] E. B. Morris, *J. Engineer for Power,* Oct. (1961) 367.
[28] K. Ogura and K. Sato, *Electrochim. Acta* **25** (1980) 857, 1227.
[29] K. Ogura and T. Ohama, *Corrosion* **38** (1982) 403.
[30] H. G. Oswin and M. Cohen, *J. Electrochem. Soc.* **104** (1957) 9.
[31] M. Pavarotti and R. Rizzi, CISE—NT Italy, Report (1982) 82.061.
[32] M. Pavarotti, R. Rizzi and C. Ronchetti, CISE — NT Italy, Report (1982) 1797; Conference on Decontamination of Nuclear Facilities, 19–22 Sept. (1982) Niagara Falls, NY.
[33] I. H. Plonski, M. Toader, F. Berevoianu and A. Cristescu, *Patent RO-OSIM* no. 97 049 (1988).
[34] I. H. Plonski, *Corrosion* 46 (1990) 581.
[35] *Idem, ibid.* **47** (1991) 840.
[36] *Idem, St. Cerc. Fiz.* **43** (1991) 233, 395.
[37] *Idem, Ber. Bunsenges. Phys. Chem.* **97** (1993) 8.
[38] *Idem, in* Proceedings of the International Conference on Energy, Environment and Electrochemistry, 10–12 Feb. (1993), Karaikudi, India, p. A-105, paper no. 4–49.
[39] *Idem, J. Radioanal. & Nucl. Chem.* **178** (1994), 359 **185** (1994) 251.
[40] *Idem, J. Mater. Sci. Forum* **185** (1995) 649.
[41] *Idem,* Effect of Surface Structure and Adsorption Phenomena on the Active Dissolution of Iron in Acid Media, in 'Modern Aspects of Electrochemistry', no. 29 (edited by J. O'M. Bockris, B. E. Conway and R. E. White), Plenum Press, New York (1996) pp. 203–319.
[42] *Idem, Int. J. Hydrogen Energy* **21** (1996) 837.
[43] P. J. Pocock and W. S. Leedy, *in* Proceedings of the 32nd International Water Conf. of the Engineers Soc. of Western Pennsylvania, Pittburg, 1971.
[44] M. Pourbaix, 'Atlas d'Equilibres Electrochimiques', Paris, Gauthier-Vilars et Cie (1963) p. 307.
[45] M. J. Pryor and U. R. Evans, *J. Chem. Soc.* (1950) 1259, 1266.
[46] M. J. Pryor, *J. Chem. Soc.* (1950) 127.
[47] R. Rizzi, CISE — NT Italy, Report (1978).
[48] T. Sava and Y. Furutany, INIS File Research, March (1989) 51.
[49] M. G. Segal and T. Swan, *in* 'Water Chemistry 3', BNES, London, (1983) p.187.
[50] D. W. Shoesmith, T. E. Rummery, Woon Lee and D. G. Owen, *Power Ind. Res.* **1** (1981) 43.
[51] D. W. Shoesmith, Woon Lee and D. G. Owen, *ibid.* **1** (1981) 253.
[52] C. D. Stockbridge, P. Sewell and M. Cohen, *J. Electrochem. Soc.* **108** (1961) 928; *ibid.* **108** (1961) 933.
[53] G. Trabanelli, F. Zucchi and A. Frignani, *Werk. Korros.* **30** (1979) 426.
[54] W. Valverde and C. Wagner, *Ber. Bunsen. Ges.* **80** (1976) 330.
[55] W. Valverde, *Ber. Bunsen. Ges.* **80** (1976) 333.
[56] D.A. Vermilyea, *J. Electrochem. Soc.* **113** (1966) 1067.
[57] K.R. Walston, *in* Corrosion'79 NACE, Atlanta (1979) paper 5.